Geomechanics and Engineering, *Vol. 41, No. 6 (2025) 625-639*
https://doi.org/10.12989/gae.2025.41.6.625

Geotechnical assessment and remediation of differential settlement in grain bins using unreinforced bored piles

Osman Sivrikaya*[1], Burak Akçay[1a], Firdevs Uysal[2b], Fatih Yesevi Okur[1c], Süleyman Adanur[1d] and Ahmet Can Altunışık[1e]

[1]*Department of Civil Engineering, Karadeniz Technical University, 61080 Trabzon, Turkey*
[2]*Department of Civil Engineering, Niğde Ömer Halisdemir University, 51240 Niğde, Turkey*

(*Received October 23, 2024, Revised April 17, 2025, Accepted June 17, 2025*)

Abstract. This paper aims to perform a stability analysis of an existing grain bin project based on the 2018 Turkish Building Earthquake Code (TBEC), and to achieve soil improvement and reinforcement solutions using unreinforced bored piles. In the study area, after the construction of the grain bins, static loading was applied, and soil problems were observed in certain sections. As a result, some grain bins were partially taken out of use. To diagnose the problem and understand the soil stratigraphy, eight (8) boreholes were drilled in the study area. The results indicated that the soil was exposed to surface water, which caused settlement problems. To solve this problem, the soil was improved by supporting it with unreinforced piles. The grain bins with capacities of 28000 kN for wheat and 24000 kN for barley, consisting of 18 storage cells with a diameter of 14 m each, located in Sarıoğlan district, Kayseri city, Turkey, were investigated in this paper. The observations of differential settlement and heave as geotechnical problems started after two of these grain bins were loaded twice with approximately 15000 kN. The extensive laboratory and field tests revealed that the soil consisted of vegetative soil, alluvial soil of various thicknesses and sandstone, in addition to the fact that the study area is close to an active fault. Bearing capacity and horizontal slip were checked according to TBEC (2018), and settlement analyses were carried out using PLAXIS 2D and 3D to identify the mechanical characteristics of the grain bins that have differential settlement problems in the field. The amount of settlement occurring in the existing condition was determined to be approximately $s_0 \cong 47$ mm. In the case of ground improvement and reinforcement, the maximum total settlement was found to be $s_1 \cong 23$ mm, the maximum differential settlement $s \cong 0.21$ mm, and the angular distortion $\cong 0.0015\%$. As a result of the investigations, it was understood that there was no bearing capacity and horizontal slip failure, and the numerical analyses indicated that the use of unreinforced bored piles with controlled embankment brought the settlement and angular distortion to permissible limits.

Keywords: grain bins; settlement; soil improvement; stability analysis; unreinforced bored piles; 2018-TBEC

1. Introduction

Geotechnical analysis plays a fundamental role in the design of safe and efficient foundations. As the structural element responsible for transferring loads to the ground, a foundation must be supported by soil or rock with adequate bearing capacity and deformation characteristics. Geotechnical design encompasses the evaluation of bearing capacity, base contact pressure, horizontal sliding resistance, and settlement behavior, particularly for shallow foundations (CFEM 2006, Das 2011, TBEC 2018).

Through detailed site investigations, geotechnical analysis provides critical data on subsurface conditions, including soil type, shear strength, stiffness, permeability, and compressibility. These parameters are essential for selecting appropriate foundation systems and identifying potential risks such as slope instability, liquefaction, and swelling. Slope stability assessments help detect areas susceptible to failure during or after construction, while liquefaction analysis evaluates how saturated, loose soils may lose strength under seismic loading. For expansive clays prone to volumetric changes due to moisture variation, mitigation techniques such as preloading or specialized deep foundations are often required to limit differential settlement (Bowles 1996, Das 2019, Sivrikaya 2021a, Sivrikaya,2021b).

Soil improvement and reinforcement techniques are commonly applied to enhance the engineering properties of existing soils. When native soils are inadequate in strength or compressibility, methods such as compaction, consolidation, preloading, or the addition of stabilizing agents (e.g., lime or cement) can be used to improve performance. These measures increase the bearing capacity

*Corresponding author, Professor
E-mail: osivrikaya@ktu.edu.tr
[a]Ph.D. Student
E-mail: burak.akcay@ktu.edu.tr
[b]Associate Professor
E-mail: firdevsuysal@ohu.edu.tr
[c]Assistant Professor
E-mail: yesevi@ktu.edu.tr
[d]Professor
E-mail: sadanur@ktu.edu.tr
[e]Professor
E-mail: ahmetcan@ktu.edu.tr

ISSN: 2005-307X (Print), 2092-6219 (Online)

and help control settlement, ensuring long-term stability. Additionally, soil improvement mitigates geotechnical hazards like liquefaction and slope failure. For example, densification through deep compaction improves the stiffness and strength of liquefiable soils, while slope stabilization can be achieved using retaining systems or grouting methods (Nicholson 2015, Ergun 2023, Sivrikaya 2021b).

In cases where significant settlement has already occurred, one effective remedial approach is the use of unreinforced bored piles. These piles transfer structural loads to deeper, more competent strata and reduce additional settlement by bypassing the weak upper layers. Compared to other techniques such as jet grouting or deep mixing, bored piles offer practical advantages for specific soil and load conditions. Their successful application depends on careful design, installation, and site-specific adaptation (Xiao *et al.* 2016, Wang *et al*. 2023, Vanni *et al*. 2018, Varaksin *et al*. 2016, Sondermann 2018).

The use of finite element method (FEM)-based programs has become increasingly widespread in geotechnical practice. FEM enables the simulation of complex soil-structure interaction and provides insight into stress distribution, deformation, and failure mechanisms under different loading conditions. PLAXIS 2D and 3D are widely adopted FEM tools designed for advanced geotechnical analysis, including modeling of consolidation, slope stability, tunneling, and foundation behavior (Potts and Zdravkovic 1999, Rao 2011, Elsawwaf *et al*. 2023). These tools support nonlinear constitutive models that simulate strain-dependent stiffness, creep, softening, and hardening behaviors, making them suitable for evaluating performance under both static and seismic conditions (Jamsawang *et al*. 2016, Dias and Grippon 2017, Alekseev and Bezvolev 2020, Zhao *et al*. 2023).

Recent studies have extensively documented the effectiveness of pile-supported embankments and other ground improvement methods. For instance, Zhang et al. (2010) proposed an analytical model to evaluate pile-soil stress ratios, while Mishra (2016) presented a comprehensive review of modern ground improvement techniques. Briançon and Simon (2017) conducted a full-scale comparison of pile-supported embankments (PE) and geogrid-reinforced piled embankments (GRPE), demonstrating that GRPE offered superior settlement reduction and load transfer. Similarly, Zhao *et al*. (2021) highlighted the seismic isolation benefits of gravel cushions through shake table experiments. These and other investigations confirm that various pile-based and ground reinforcement methods, supported by numerical modeling, can significantly improve foundation performance (Ambily and Gandhi 2007, Başköse and Gökçeoğlu 2019, Tipsunavee *et al*. 2023, Can *et al*. 2024).

In this study, a geotechnical problem involving settlement of grain bins in Sarıoğlan, Kayseri, Türkiye was investigated. A remediation solution combining controlled granular embankment and unreinforced bored piles was developed. The analysis was carried out using theoretical design principles in accordance with TBEC (2018) and advanced FEM-based tools. The methodology adopted in this research is summarized in the flowchart shown in Fig. 2.

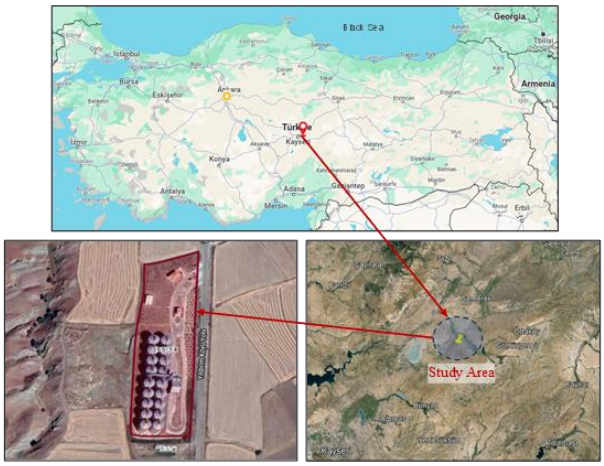

Fig. 1 Location map of the study area

2. Characteristics of the site and grain bins

2.1. General information

The study site is located in the Sarıoğlan District of Kayseri Province in the Central Anatolia Region of Türkiye, covering an area of approximately 26,300 m². The facility includes 18 cylindrical grain bins and related buildings arranged in two parallel rows (Fig. 1). The site has a natural ground slope of about 5–6% and is bordered by vacant parcels with no adjacent structures, allowing for unobstructed access during site investigation, monitoring, and remediation activities.

Each grain bin, constructed from steel, has a height of 20 meters and a diameter of 14 meters. The storage capacity is 28,000 kN for wheat and 24,000 kN for barley (Fig. 3). In accordance with the 2018 Turkish Building Earthquake Code (TBEC), the grain bins are classified under Building Usage Class (BUC) 3, with a Building Importance Coefficient (I) of 1.0.

2.2 Regional geology

Kayseri Province, located in the Central Anatolia Region of Türkiye, is bordered by Kahramanmaraş to the east, Nevşehir to the west, Yozgat to the north, and Adana to the south (Fig. 2). The region has a complex geological structure composed of rock assemblages from various geological periods and environments, primarily shaped by the Alpine orogeny. It features igneous, metamorphic, and sedimentary massifs, with Paleozoic and Lower Mesozoic formations predominantly formed through metamorphic processes (Ketin 1959). In the study area, Quaternary alluvium, as well as peridotite and gabbro formations, are commonly observed. Geomorphologically, the site is situated within a closed basin characteristic of arid region topography (Özlü *et al*, 2017). The area is subject to geomorphological hazards such as flooding, mass movements, wind erosion, and salinization, all of which

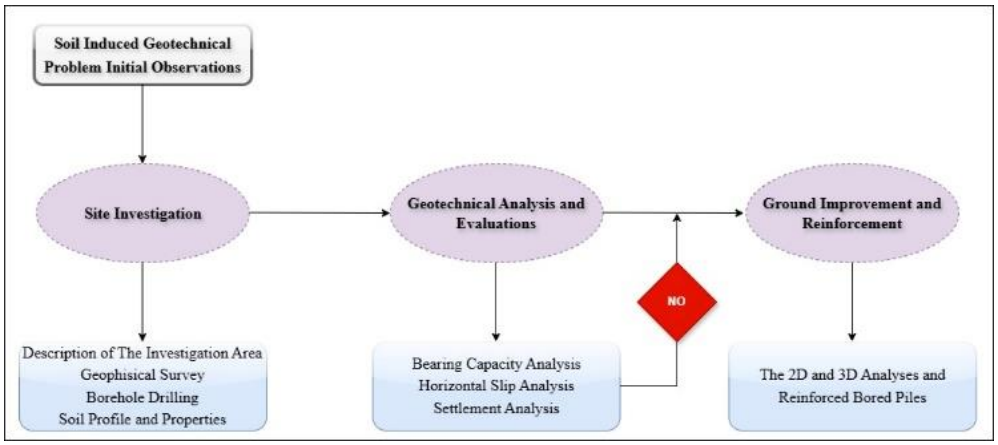

Fig. 2 Flowchart of the methodology

Fig. 3 Layout plan and general view of grain bins

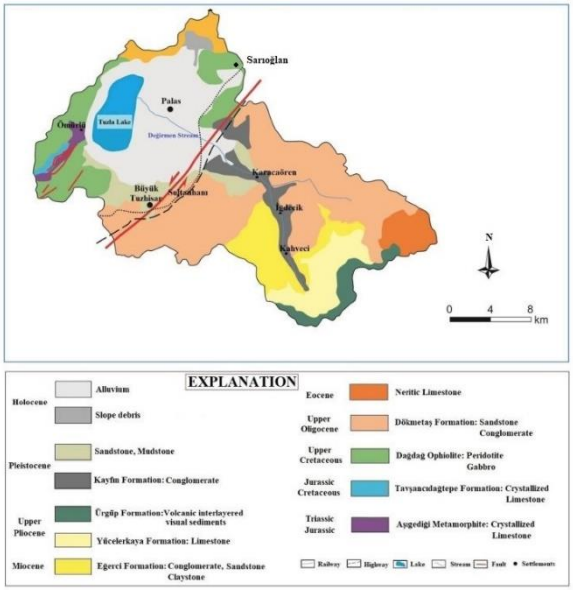

Fig. 4 Geological map of the region (Özlü and Gündüz, 2018)

contribute to ongoing economic challenges. Tectonically, Kayseri and its surroundings are of significant importance, lying along the active Ecemiş fault zone and associated fault systems, which are critical to the seismicity of the region. The province experiences a continental climate with precipitation occurring mainly during winter, spring, and autumn, while summers are typically dry. The average annual precipitation is approximately 345.32 mm (IRAP 2021).

2.3 Soil investigation

Soil investigation activities and on-site observations were incorporated into the geotechnical evaluation of the study area. The natural topographic slope across the grain bin site ranges from 0 to 5 percent. After the two major earthquakes that struck southern Türkiye on February 6, 2023, with magnitudes of Mw 7.7 at 4:17 a.m. and Mw 7.6 approximately nine hours later, visual inspections confirmed that no slope stability issues were present at the site.

To determine the subsurface conditions and soil parameters, eight boreholes were drilled in total. Seven were advanced to a depth of 10 meters and one to a depth of 5 meters. The boreholes were concentrated around the grain bins, particularly in areas where settlement was observed (Fig. 5). Field inspections showed that grain bin S-10 had experienced settlement of approximately 40 to 50 millimeters in the southeast direction, along with slight heaving behind it (Figs. 3 and 5). The soil profile consists of a vegetative layer at the surface, followed by alluvial deposits of varying thickness, and a sandstone layer at greater depth.

Disturbed and undisturbed soil samples were collected during drilling, and laboratory tests were conducted in accordance with ASTM standards to determine water content, consistency limits, natural unit weight, shear strength parameters, and consolidation characteristics. Since the sandstone layer is classified as rock, core samples were extracted and tested using point load testing to evaluate its strength. Standard Penetration Tests (SPT) were performed in all boreholes to assess in-situ soil resistance. Additionally, two seismic refraction surveys, two Multi-Channel Analyses of Surface Waves (MASW), and three electrical resistivity tomography (ERT) tests were carried

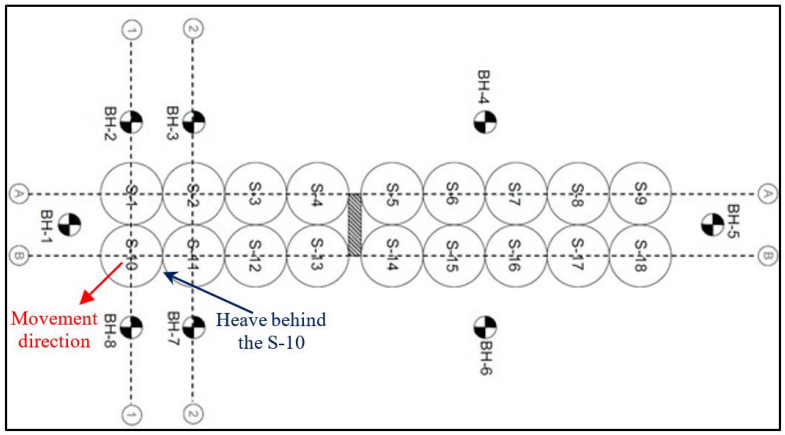

Fig. 5 Locations of the grain bins, boreholes (BH), and sections (1-1, 2-2, A-A, B-B)

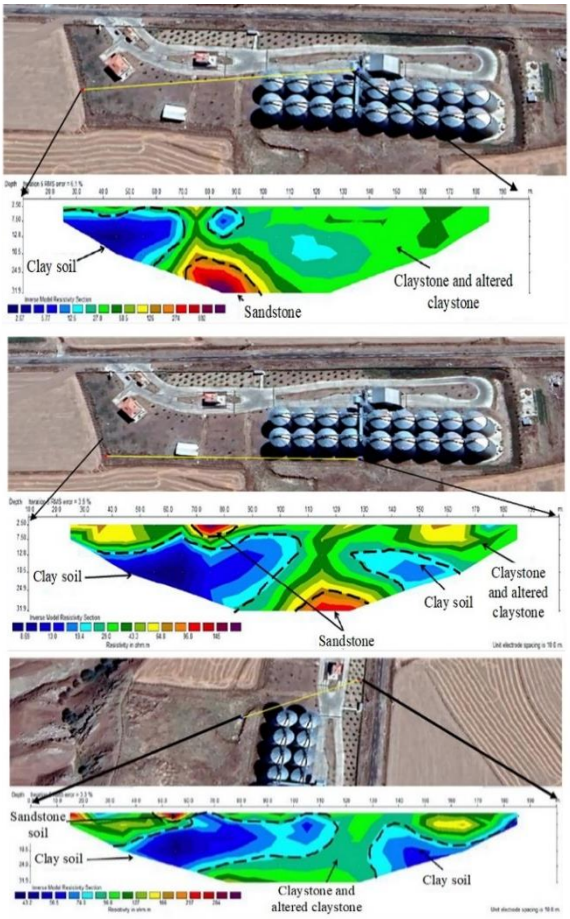

Fig. 6 Results of ERT with tomography

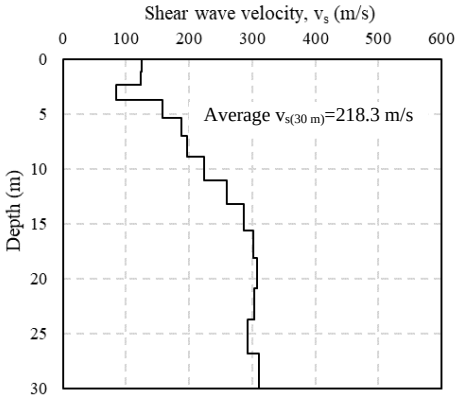

Fig. 7 Variation of shear wave velocity with depth

out to evaluate the geophysical properties of the subsurface layers (Figs. 6 and 7).

2.4 Soil profile and properties

Subsurface investigations revealed that the local geological formation, known as the İncik Formation, consists of a surface layer of approximately 0.30 meters of vegetative soil, underlain by alluvial deposits of variable thickness depending on borehole location, followed by a sandstone layer at greater depth. Groundwater was not encountered during borehole drilling or geophysical studies. Additionally, no irrigation channels or nearby surface water bodies such as lakes or streams were present that could influence subsurface moisture conditions.

According to the Unified Soil Classification System (USCS), the alluvial soils were classified as CL (low-plasticity clay), SC (clayey sand), SM (silty sand), and GC (clayey gravel). The idealized subsurface profile developed from borehole logs and geophysical testing is shown in Fig. 8 for cross sections A–A, B–B, 1–1, and 2–2. For the purposes of modeling and analysis, it was assumed that the geotechnical properties within the CL zone were consistent throughout, and this layer was identified as the most critical in the profile. The underlying sandstone forms the second layer and serves as a more competent bearing stratum. The first layer of soil, classified as CL (low-plasticity clay), lies beneath the stripped vegetative layer and forms part of the foundation soil depending on the location. Laboratory tests indicated a water content of approximately 12 percent, a liquid limit of 38 percent, and a plastic limit of 20 percent. The unit volume weight of this layer was measured as 17 kN/m^3. The shear strength parameters were c_u=50 kPa and ϕ_u=7° for the undrained condition and c'=8 kPa and ϕ'=28° for the drained condition. The SPT-N value was determined as 18~50 and R (refusal). The second layer is sandstone and constitutes the foundation unit built on the grain bin foundation, depending on the location. The sandstone layer

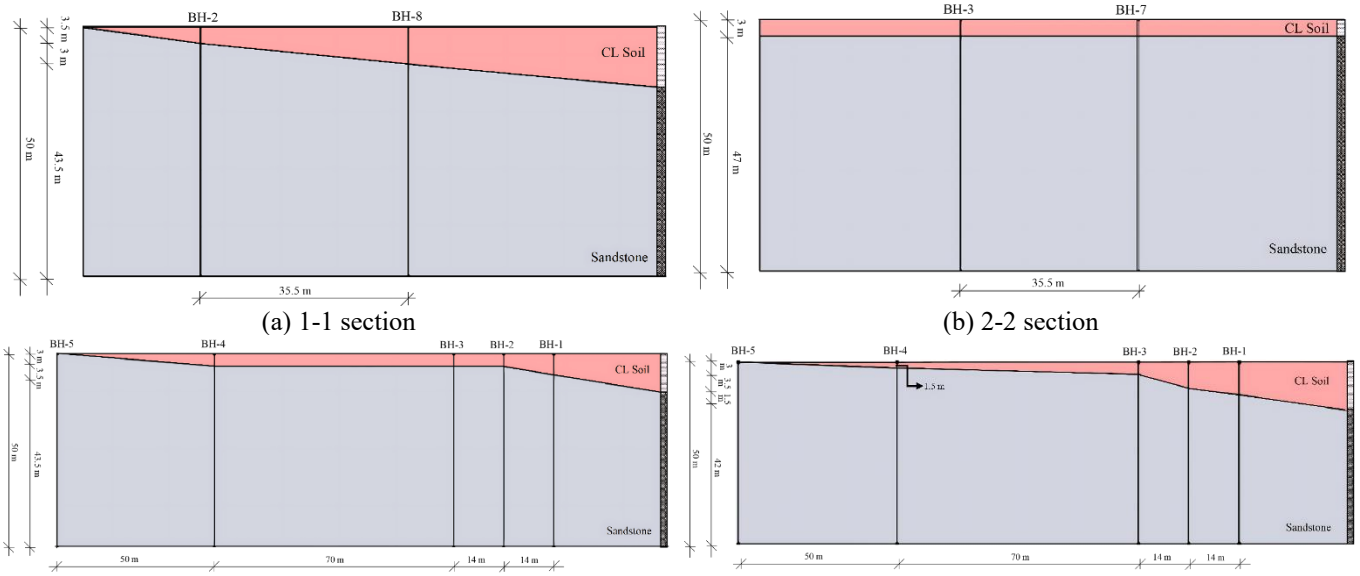

(a) 1-1 section (b) 2-2 section

(c) A-A section (d) B-B section

Fig. 8 Idealized soil profiles used in the analyses

had a TCR=31~45%, SCR=19~33%, RQD=16~28%, unit volume weight of approximately γ=21kN/m^3. It also had a weathering degree as moderately weathered, crack frequency as frequent, and rock strength as weak. The foundation soil of 30 m deep had the shear wave velocity of v_{30}=218.3 m/s.

At the site where the grain bins are located, a low-plasticity clay (CL) layer was encountered at varying depths beneath the surface vegetative soil in all boreholes. Underlying this layer, weathered sandstone was observed at different depths depending on location. Core samples extracted from the sandstone were subjected to point load testing, yielding an average point load strength index (I_{s50}) of 727 kPa. Using empirical correlations, the uniaxial compressive strength of the rock was estimated as q_{ur} = 12 MPa based on the I_{s50} value. Additionally, the internal friction angle (ϕ) of the weathered sandstone was estimated using empirical relationships from the literature, treating the material as a granular medium due to its degree of weathering.

The geotechnical design parameters for both the low-plasticity clay and the weathered sandstone are summarized in Table 1. Based on the measured shear wave velocity, the site was classified as Local Soil Class ZD in accordance with the 2018 Turkish Building Earthquake Code (TBEC).

Table 1 Geotechnical design parameters of the foundation soils

Model and Soil Parameters	CL	Sandstone
Soil model	Hardening Soil	Hardening Soil
Drainage type	Drained	Drained
γ_{unsat} (kN/m^3)	17	21
γ_{sat} (kN/m^3)	18	22
$E'_{50}{}^{ref}$=$E'_{oed}{}^{ref}$ (MPa)	15	120
$E'_{ur}{}^{ref}$ (MPa)	45	360
ν'_{ur}	0.35	0.3
power (m)	1	0.5
ρ_{ref} (kPa)	100	100
c'_{ref} (kPa)	8	1
ϕ' (°)	28	38
ψ (°)	0	4
R_{inter}	1	0.7

2.5 Seismicity

The grain bin site, located in Sarıoğlan within the Kayseri Province of Central Anatolia, Türkiye, lies in a geologically complex and tectonically active region. This area is part of a seismically sensitive zone influenced by multiple fault systems. One of the most significant of these is the North Anatolian Fault (NAF), a major strike-slip fault extending from eastern to western Türkiye, as shown in Fig. 9(a). The NAF accommodates the relative motion between the Eurasian and Anatolian tectonic plates and is a primary source of seismic hazard in the region. Historically, it has generated several large-magnitude earthquakes, including the 1939 Erzincan and 1999 İzmit events. In addition to the NAF, smaller-scale local fault systems exist throughout the Kayseri region, contributing to regional seismicity and the potential for localized ground shaking (Tatar 2000, Kocyigit and Erol 2001, IRAP 2021).

Between 1960 and 2024, numerous earthquakes with magnitudes greater than M_w 3.5 were recorded within a 100-kilometer radius of the grain bin site. The distribution of these events by magnitude and depth is illustrated in Fig. 9b (URL-1). The largest recorded earthquake in this region occurred approximately 4 kilometers from Sarıoğlan, with a magnitude of M_w 5.2. The grain bins are located just 2.6 kilometers from the nearest active fault. Given the proximity of the site to active fault zones capable of producing small to moderate or even large-scale seismic events in the future, strict adherence to the seismic

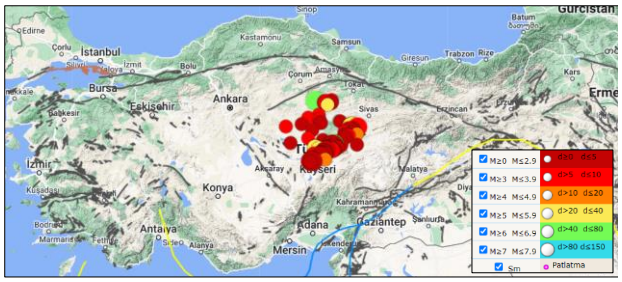

(a) Regional fault lines and recorded seismic events across Central and Eastern Türkiye are shown, highlighting the tectonic activity near the Kayseri region

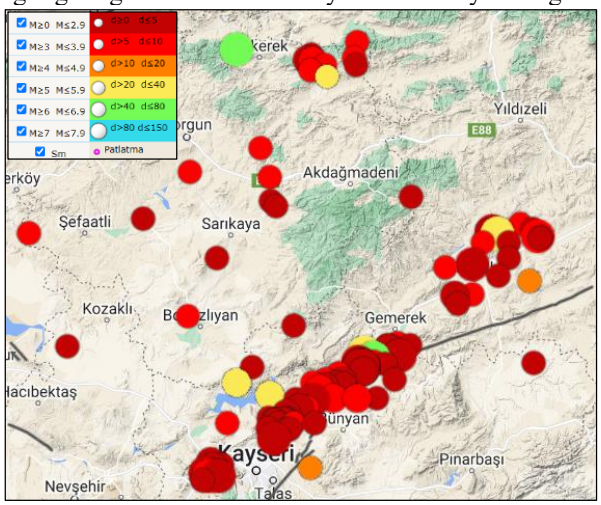

(b) A closer view of the Kayseri area shows th concentration and magnitude of local earthquakes i proximity to the grain bin site

Fig. 9 Fault lines and seismic activity in the regio surrounding the grain bins (URL-1)

provisions of the 2018 Turkish Building Earthquake Code (TBEC) is essential in any design or remedial work performed on the parcel. In accordance with TBEC (2018), earthquake design parameters were determined using the site's geographic coordinates, Earthquake Ground Motion Level DD-2, and Local Soil Class ZD, as summarized in Table 2.

Since no groundwater was encountered during borehole drilling or geophysical testing, the risk of soil liquefaction is considered negligible. Furthermore, no signs of liquefaction were observed during post-earthquake visual inspections at the site following the two major seismic events in the region.

3. Geotechnical analyses and evaluations

Each of the 18 grain bins is supported by a circular ring (strip) foundation system. The outer diameter of the foundation is 14.00 meters, while the inner diameter is 9.75 meters. The width, depth, and thickness of the strip foundation are 2.125 meters, 2.15 meters, and 0.60 meters, respectively, as illustrated in Fig. 11. To evaluate the structural response of the foundations under loading, numerical simulations were carried out using PLAXIS 2D

Table 2 Seismic design parameters

Maximum ground acceleration ($a_{h,max}$)	0.235 g
Design spectral acceleration coefficient for short short-period region (S_{DS})	0.739
Design spectral acceleration coefficient for 1.0 second period (S_{D1})	0.333
Horizontal elastic design acceleration spectrum corner periods (T_A, T_B, T_L)	0.090 s, 0.451 s, 6 s
Vertical elastic design acceleration spectrum corner periods (T_{AD}, T_{BD}, T_{LD})	0.030 s, 0.150 s, 3 s

and 3D finite element software. Separate models were developed for each of the cross-sections identified in Fig. 5 (A–A, B–B, 1–1, and 2–2). An idealized soil profile, based on borehole and geophysical data, was used in all models. Contact base pressures (q_0) from the grain bins were applied as distributed loads on the foundation rings. The resulting stress distribution, settlement, and deformation patterns were analyzed to assess geotechnical performance under both current and operational loading conditions.

3.1 Bearing capacity analysis

Bearing capacity analysis of the grain bins was conducted using the IdeStatik (2020) finite element program, incorporating seismic parameters in line with the 2018 TBEC, including Earthquake Ground Motion Level DD-2, Local Soil Class ZD, and a vertical subgrade reaction coefficient of k=34,000 kN/m^3. The contact (base) pressures (q_0) were calculated based on the combined dead weight of the steel grain bin and foundation (1,840 kN) and the full operational load of 28,000 kN. Both static and dynamic loading scenarios were analyzed, and the resulting base pressure distributions are presented in Fig. 10, with summary results provided in Table 3.

The allowable bearing capacity (q_a) of the problematic grain bin S-10 was calculated according to 2018 Turkish Building Earthquake Code (TBEC). Bearing capacity factors were determined using the equations and coefficients recommended by TBEC (2018), while additional parameters such as shape, depth, and load inclination factors were evaluated based on the widely accepted empirical relationships proposed by Vesic (1973, 1975). Using these inputs, the allowable bearing capacity for the foundation was calculated as q_a=628kPa.

$$q_u = cN_c s_c d_c i_c g_c b_c + \sigma_v' N_q s_q d_q i_q g_q b_q + 0.5\gamma B' N_\gamma s_\gamma d_\gamma i_\gamma g_\gamma b_\gamma \quad (1)$$

$$q_a = \frac{q_u}{\gamma_{Rv}} \quad (2)$$

where c is cohesion, γ is unit volume weight of soil, D_f is foundation depth, N_c N_q N_γ is bearing capacity coefficients, s_c s_q s_γ is shape coefficients, d_c d_q d_γ is depth coefficients, i_c i_q i_γ is load inclination coefficients, b_c b_q b_γ is foundation base inclination coefficients, g_c g_q g_γ is slope inclination coefficients, q_u is the ultimate bearing capacity and γ_{RV}=1.4 is the factor of safety.

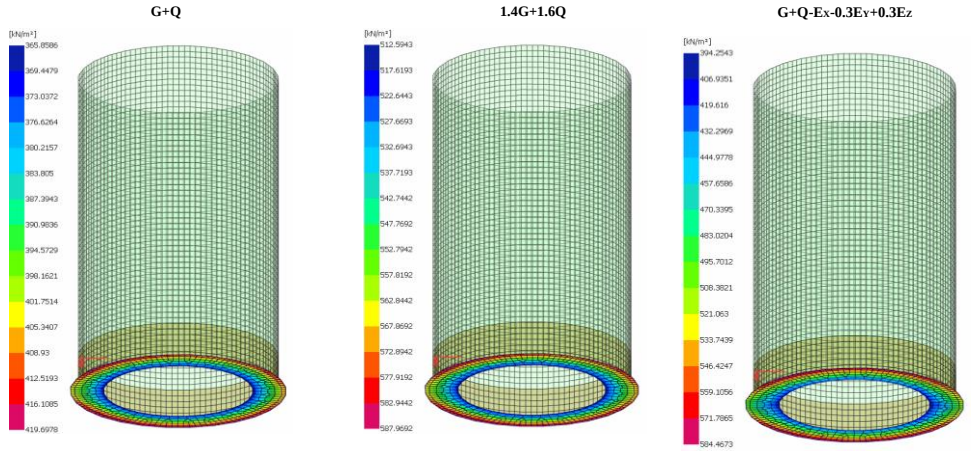

Fig. 10 Foundation base pressure distribution of the grain bin

Table 3 Results of structural analyses

Loading Type		G+Q			1.4G+1.6Q			G+Q+E/0.9G+E		
		Max.	Min.	Aver.	Max.	Min.	Aver.	Max.	Min.	Aver.
Base pressure, q_0 (kPa)		373.1	405.9	428.0	522.7	568.7	599.6	216.6	519.6	596.0
Foundation base total area, A (m^2)						77.84				
V_{th} (kN)	$V_{th,X}$					4595.4				
	$V_{th,Y}$					4595.4				

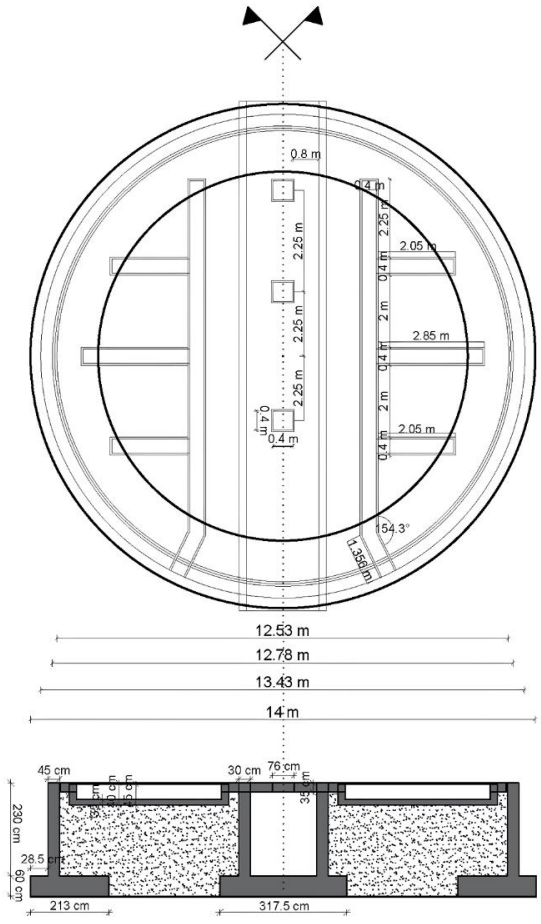

Fig. 11 Foundation system detail of the grain bin

Since the maximum base pressure exerted under the grain bins (q_0 = 599.6 kPa) is less than the calculated allowable bearing capacity (q_a = 628 kPa), the foundation soil is deemed sufficient to safely support the structural load. Furthermore, post-earthquake visual inspections conducted after the two major seismic events confirmed that no signs of bearing capacity failure were observed at the grain bin foundations.

3.2 Horizontal slip analysis

In accordance with the 2018 Turkish Building Earthquake Code (TBEC), the condition $V_{th} \leq R_{th}+0.3R_{pt}$ must be satisfied to verify the horizontal sliding resistance of shallow foundations. This check is particularly relevant for cohesive soils. The relevant soil-induced lateral forces acting on the foundation system were evaluated, and the corresponding force distribution is illustrated in Fig. 12.

$$R_{th} = \frac{c_u \times A}{\gamma_{Rh}} \tag{3}$$

$$P_p = \frac{1}{2}\gamma D_f^2 K_p \tag{4}$$

$$R_{pt} = \frac{R_{pk}}{\gamma_{Rp}} \tag{5}$$

$$R_{pt} = \frac{R_{pk}}{\gamma_{Rp}} \tag{6}$$

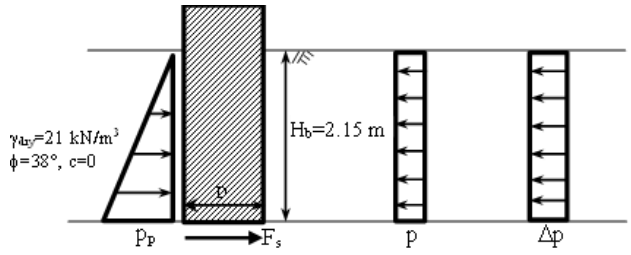

Fig. 12 Soil-induced lateral pressures and forces acting on the grain bin

$$p = 0.2 \times (\gamma H_b + q) \tag{6}$$

$$\Delta p = 0.4 S_{DS} \gamma H_b \tag{7}$$

where Vth is designed horizontal force acting on the foundation base, R_{th} is designed frictional resistance, R_{pt} is designed passive resistance, R_{pk} is characteristic passive resistance, γ_{Rh}=1.1 is frictional resistance strength coefficient, γ_{Rp}=1.4 is passive resistance strength coefficient, cu is undrained shear strength of the foundation soil, A is foundation base total area, pp is passive lateral soil pressure, p is static lateral soil pressure, Δp is additional soil pressures under earthquake, H_b is basement depth, S_{DS} is short period design spectral acceleration coefficient, q is surcharge load.

The horizontal sliding safety check was satisfied, as shown in Eq. (8), confirming that no slippage occurs at the soil–foundation interface under the applied design loads. Furthermore, post-earthquake visual inspections conducted after the two major seismic events in the region revealed no evidence of horizontal slip failure in the structures.

$$V_{th} = 4483 \text{ kN} \le R_{th} + 0.3 R_{pt} = 5460 \text{ kN} \tag{8}$$

3.3 Settlement analysis

The foundation soils beneath grain bins S-1, S-2, S-10, and S-11 are primarily composed of low-plasticity clay, which is known to exhibit significant reductions in shear strength and stiffness upon exposure to water. Although groundwater was not encountered in the boreholes, geotechnical evidence and field behavior confirm that differential settlement occurred as a result of softening in an approximately 7-meter-thick clay layer located beneath inadequately drained areas. During two loading sequences of approximately 15,000 kN applied to the currently empty S-1 and S-10 grain bins, measurable displacement and settlement were observed in S-10. This displacement was directed toward the southeast, consistent with the site slope and stratigraphy, as shown in Fig. 5. In addition, visible relative movement between S-10 and S-11 was recorded during site inspections (Fig. 3). These findings, supported by structural response and deformation patterns, led to the decision to unload both S-1 and S-10 to prevent further damage or instability.

To quantify these deformations and validate the failure mechanism, numerical simulations were performed using PLAXIS 2D and 3D finite element software. The analyses incorporated an idealized subsurface model consisting of soft clay overlying weathered sandstone, aligned with site-specific borehole and laboratory data. Appropriate constitutive models were used to simulate nonlinear stress-strain behavior under staged loading. Displacement evaluations were conducted for four representative cross-sections: A to A, B to B, 1 to 1, and 2 to 2. Among these, Sections 1 to 1 and B to B exhibited the most critical behavior based on stratigraphic conditions and observed field performance. The 2D and 3D model results clearly reflect the deformation trends seen in the field, and displacement distributions are presented in Figs. 13 and 14, and Figs. 15 and 16, respectively.

The results of the analyses of the 2D models in terms of displacement are shown in Figs. 13 and 14. For the 1-1 section, the distributions of the horizontal displacement, vertical displacement (settlement), and equivalent displacement are presented in Fig. 13, and the maximum horizontal displacement, maximum vertical displacement (settlement), and equivalent maximum displacement were found to be as u_x=11.2 mm, u_y=53.27 mm and |u|=53.35 mm, respectively.

For the B-B section, the distributions of the horizontal displacement, vertical displacement (settlement), and equivalent displacement are presented in Fig. 14, and the maximum horizontal displacement, maximum vertical displacement (settlement), and equivalent maximum displacement were found to be as u_x=27.51 mm, u_y=127.2 mm and |u|=127.3 mm, respectively.

In the 3D analyses, the displacements in the horizontal (x and y) and vertical (z) axes were also determined for the sections (A-A, B-B, 1-1, and 2-2) and are shown for the critical sections (1-1 and B-B) in Figs. 15-16. For the 1-1 section, the distributions of the horizontal displacements, vertical displacement (settlement), and equivalent displacement are presented in Fig. 15, and the maximum horizontal displacements in the x-axis and y-axis, maximum maximum vertical displacement (settlement) in the z-axis and equivalent maximum displacement were found to be as u_x=6.12 mm, u_y=1.84 mm, u_z=46.8 mm and |u|=46.86 mm, respectively. The settlement distribution and direction obtained from the 3D analysis in terms of all grain bins are shown in Fig. 17 and the maximum total settlement (equivalent displacement) was found to be as |u|=48.54 mm.

The maximum displacements obtained from the 2D and 3D finite element analyses are summarized in Table 4. As expected, the 2D analysis results produced slightly higher displacement values compared to the 3D results. This is attributed to geometric simplifications and the absence of confinement effects that are inherently captured in 3D modeling. Furthermore, the numerical models were intentionally developed using conservative assumptions, such as simplifying the complex and heterogeneous subsurface conditions into idealized stratified layers. Therefore, the actual displacements observed in the field are expected to be slightly lower than the calculated values. The maximum displacements obtained from the 2D and 3D simulations are presented in Table 4. Displacements in the 2D analysis were marginally higher due to geometric simplifications and inherent scale effects. The model

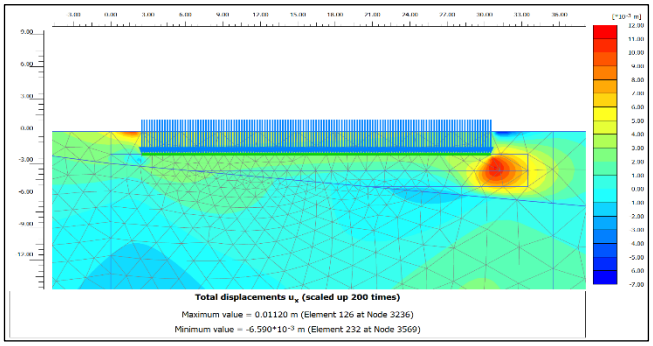

(a) u_x

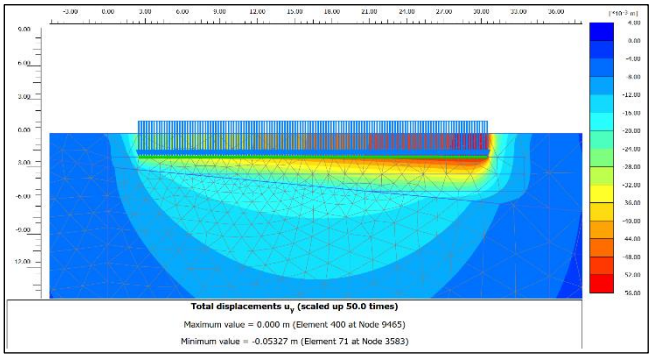

(b) u_y

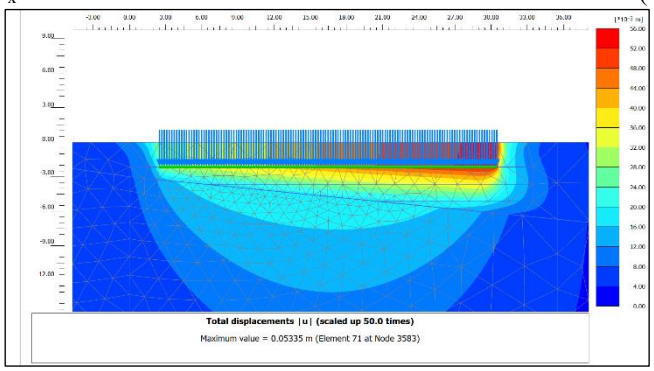

(c) |u|

Fig. 13 2D analyses and displacements were obtained for the section 1-1

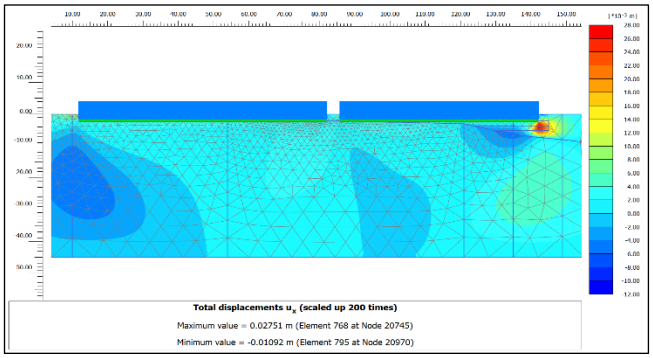

(a) u_x

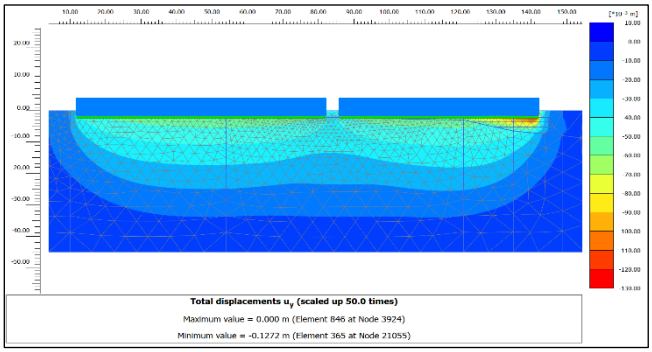

(b) u_y

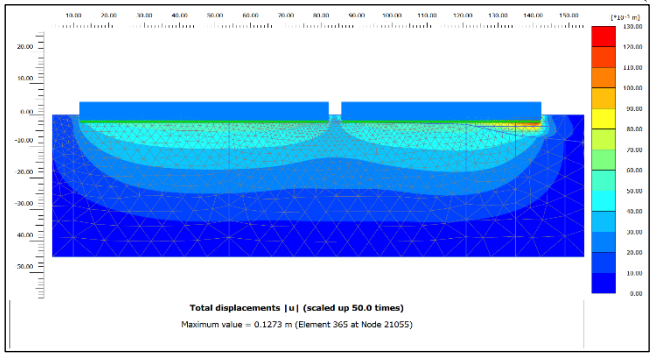

(c) |u|

Fig. 14 2D analyses and displacements were obtained for the section B-B

incorporated stratigraphic heterogeneity and utilized conservative input parameters based on field and laboratory data. Observational evidence from the site indicated southeast-directed movements of 40–50 mm beneath bin S-10, consistent with predicted results (Table 4, Fig. 17). These displacements were attributed to differential

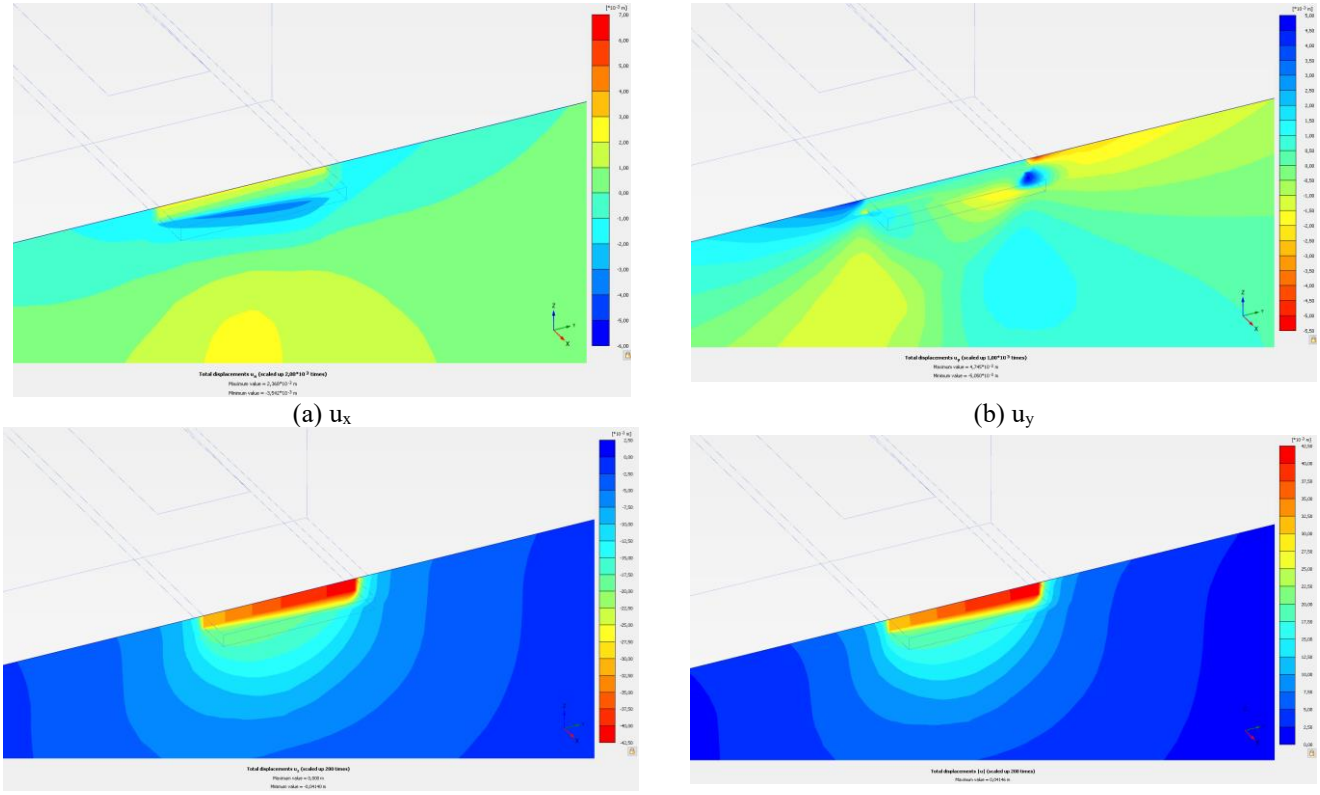

(a) u_x (b) u_y

(c) u_z (d) $|u|$

Fig. 15 3D analyses and displacements were obtained for the section 1-1

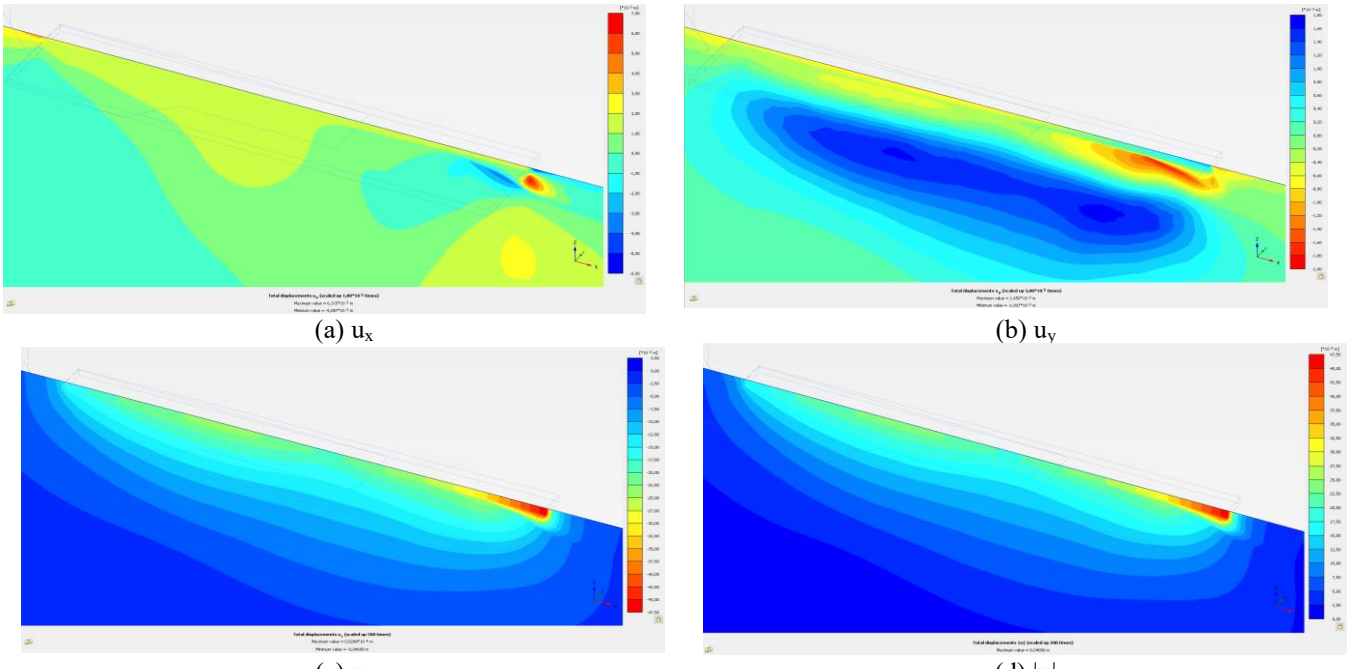

(a) u_x (b) u_y

(c) u_z (d) $|u|$

Fig. 16 3D analyses and displacements were obtained for the section B-B

compressibility in the underlying clay stratum (identified through subsurface exploration), which was explicitly modeled. The directional agreement and magnitude correlation validate the model's credibility as a diagnostic and predictive tool.

Field inspections confirmed displacement magnitudes in the range of 40 to 50 millimeters toward the southeast, which were evaluated through visual and observational methods. Table 4 and Fig. 17 demonstrate that the direction of displacement determined from the numerical analyses is consistent with field observations. This directional

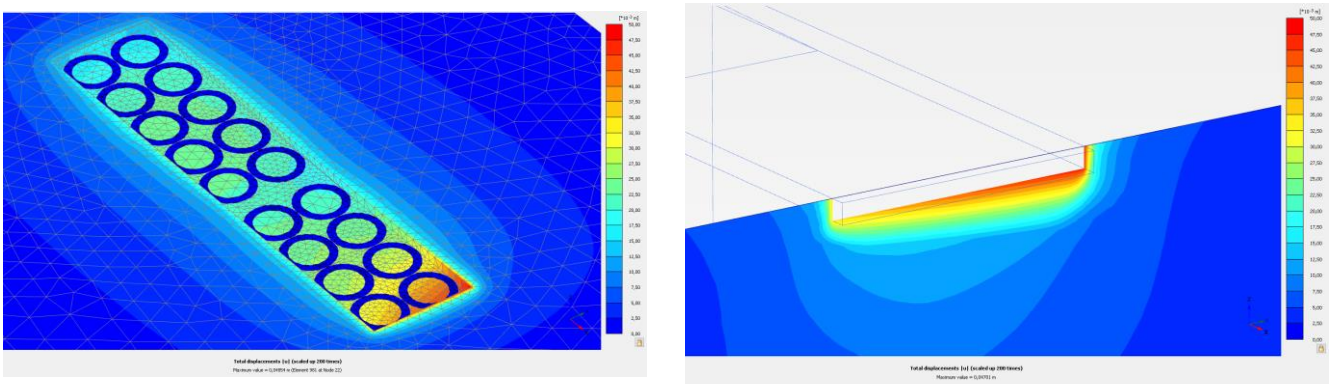

Fig. 17 Settlement distribution and direction obtained from the 3D analyses

Table 4 Results of structural analyses

2D Analyses			
	ux (mm)	uy (mm)	|u| (mm)
Section 1-1	11.2	53.27	53.35
Section 2-2	5.99	29.91	29.91
Section A-A	12.55	72.65	72.66
Section B-B	27.51	127.2	127.3

3D Analyses				
	ux (mm)	uy (mm)	uz (mm)	|u| (mm)
Section 1-1	3.54	4.75	41.4	41.46
Section 2-2	1.85	4.74	29.43	29.46
Section A-A	5.21	1.85	40.42	40.49
Section B-B	6.12	1.84	46.8	46.86

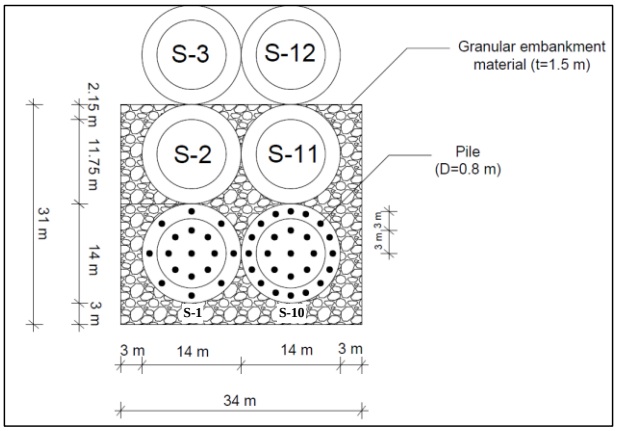

Fig. 18 View of the granular embankment and unreinforced bored piles

movement corresponds with the location of the S-10 grain bin, which is situated above a thick, compressible clay layer, as shown in Fig. 3.

The results from both 2D and 3D analyses indicate that horizontal displacements are minimal and within negligible limits, while vertical displacements are significant. These findings confirm that vertical settlement is the dominant deformation mode affecting the foundation system. The root cause of the excessive settlement is attributed to the softening of the subgrade clay due to surface water accumulation, a consequence of inadequate surface and rainfall drainage. It is therefore essential to implement soil improvement and drainage control measures to mitigate further vertical deformation.

3.4 Ground improvement and reinforcement

Based on the results of the numerical analyses and geotechnical evaluations, it is recommended that the S-1, S-2, S-10, and S-11 grain bins be temporarily dismantled to facilitate subgrade improvement. Excavation should be performed to a depth of approximately 1.5 meters below the foundation base. Within this zone, a compacted granular embankment layer with a thickness of 1.5 meters should be placed using controlled placement and compaction techniques. To improve load distribution and mitigate potential punching shear failure due to concentrated vertical stresses from the foundation, the granular fill should be extended laterally by 3 meters beyond the foundation edge, as illustrated in Fig. 18.

The granular embankment material was determined as well-graded gravel (GW) according to the USCS method. The unit weight and the angle of internal friction of the granular embankment material were determined as γ=21 kN/m^3 and ϕ=40°, respectively.

In addition to the granular backfill, support for bins S-1 and S-10, which show signs of ground motion, must also involve unreinforced bored columns with a circular cross-section of 0.8 m. A total of 42 such columns will limit soil strain and allow vertical distortion to stay within functional limits. Columns must start at the base of the granular backfill and go down into firm sandstone for at least 3 m. Columns will follow after the initial cut to 2.15 m and backfill of 1.5 m, totaling 3.65 m of initial work. Column layouts and draft shaft depths can vary; all must anchor into hard rock by no less than 3 m, as listed in Table 5.

Workflow for this mitigation is as follows:

- The S-1, S-2, S-10, and S-11 grain bins and foundation systems should be removed.
- 1.5m of clay soil should be excavated.
- For the grain bins S-1 and S-10, 0.80m diameter unreinforced bored piles should be constructed as shown in Figs. 19 and 20, penetrating 3 m into the sandstone (outer piles should be placed directly under the strip foundation).

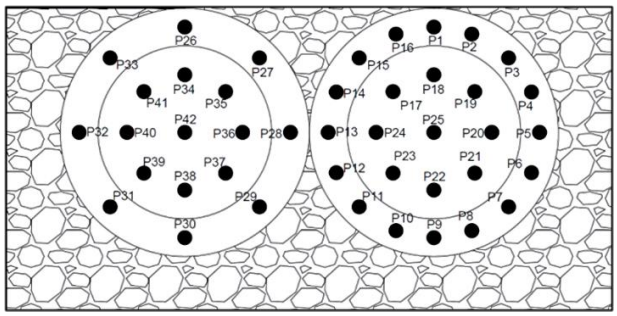

Fig. 19 Unreinforced bored piles in a plan view

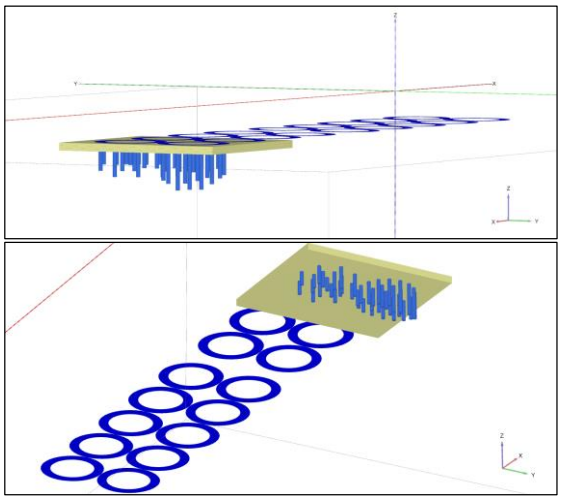

Fig. 20 3D view of unreinforced bored piles and granular embankment

Table 5 Lengths of unreinforced bored piles

Pile	Length (m)	Pile	Length (m)
P1	3.0	P22	6.0
P2	3.5	P23	5.0
P3	40.	P24	4.0
P4	4.5	P25	4.0
P5	5.0	P26	3.0
P6	6.0	P27	3.0
P7	7.0	P28	3.5
P8	7.0	P29	5.0
P9	7.2	P30	5.0
P10	6.0	P31	4.0
P11	5.5	P32	3.0
P12	5.0	P33	3.0
P13	4.0	P34	3.0
P14	3.5	P35	3.0
P15	3.0	P36	3.5
P16	3.0	P37	4.0
P17	4.0	P38	4.0
P18	3.5	P39	3.5
P19	4.0	P40	3.0
P20	5.0	P41	3.0
P21	5.5	P42	3.0

- 1.5 m GW soil should be laid and compacted in a 0.30 m thickness, and a controlled embankment should be constructed (Figs. 18-20).
- The strip foundation system of the S-1, S-2, S-10, and S-11 grain bins should be remanufactured, and for the S-1 and S-10 grain bins, the outer piles should be manufactured in such a way that the base of the strip foundation is centered and placed exactly on the piles.
- The removed grain bins (S-1, S-2, S-10, and S-11) should be remanufactured.

The locations of the unreinforced bored piles to be manufactured and granular embankment material are shown in Figs. 18 and 19 and the 3D view of the piles and granular embankment is shown in Fig. 20. The length of each pile, whose locations are given and named in Fig. 18, is given in Table 5.

3D modeling was performed to assess the effects of ground improvement and foundation reinforcement. The results of the analyses are presented in Fig. 21. The simulations validated the observed damage mechanisms and provided a basis for evaluating potential retrofitting strategies for the affected grain bins. In the improved soil condition, the maximum equivalent displacement (settlement) was calculated as approximately 25.14 millimeters. In the vicinity of grain bin S-10, identified as the critical location based on field evidence, the equivalent displacement was found to be slightly lower, with a maximum value of 23.45 millimeters.

These displacement values were obtained using a conservative modeling approach that simplifies the actual subsurface complexity into idealized soil layers. As a result, the settlement values expected to occur under improved conditions in the field are likely to be lower than those predicted in the numerical model.

According to the results obtained from finite element analysis (FEA) incorporating the proposed soil improvement strategy, the deformations were effectively reduced, with total settlements limited to approximately 20 millimeters. Furthermore, settlement at the foundation of the S-10 grain bin was found to be nearly uniform. The maximum differential settlement was calculated as approximately $\Delta s \cong 0.21$millimeters, and the corresponding angular distortion was $\beta \cong 0.0015$ percent—both of which remain well within acceptable serviceability limits (Fig. 21).

Although the existing circular strip (ring) foundation satisfies the bearing capacity and horizontal sliding requirements, the S-10 grain bin exhibited excessive settlement under loading. To address this, a ground improvement solution is proposed: a 1.5-meter-thick controlled granular embankment beneath grain bins S-1, S-2, S-10, and S-11, and the installation of unreinforced bored piles beneath the embankment for bins S-1 and S-10. The compacted embankment layer will act as a seismic isolator, attenuating dynamic loads and minimizing stress transmission to the underlying piles during seismic events, especially considering the elevated structure height of the grain bins.

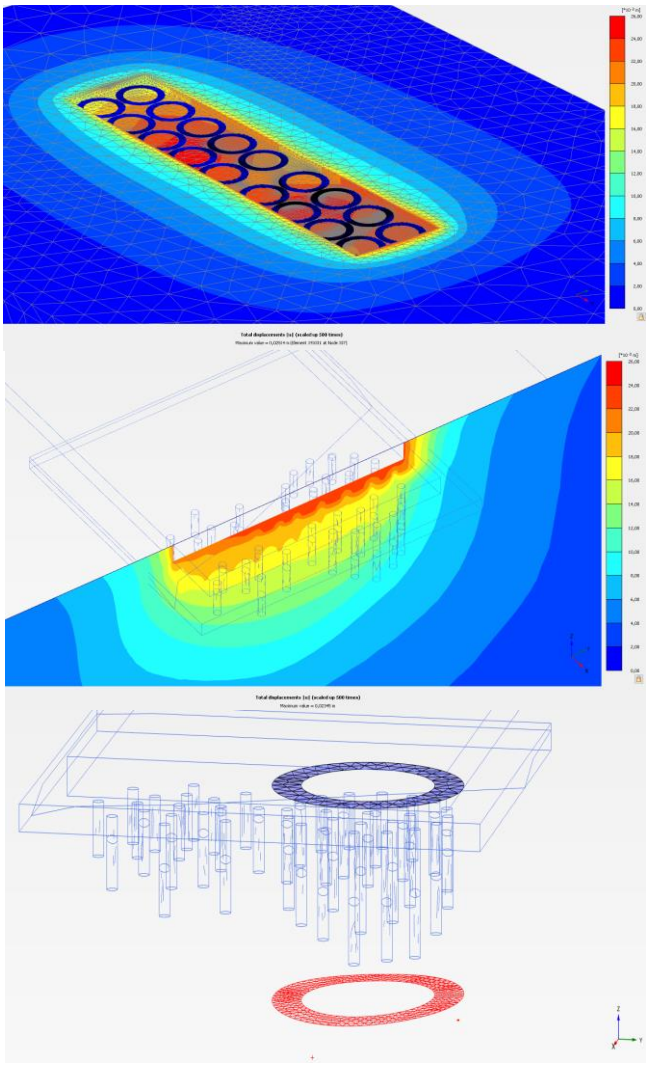

Fig. 21 3D analysis and displacement

4. Conclusions

A total of 18 grain bins were constructed for storage purposes in Sarıoğlan, Kayseri, Türkiye. Among them, grain bins S-1 and S-10 were subjected to two loading cycles of approximately 15,000 kN. Following these loadings, noticeable displacements were observed, and heaving occurred between bins S-10 and S-11 due to differential settlement. The S-1 and S-10 grain bins were subsequently unloaded. To identify the underlying causes and develop appropriate remediation strategies, detailed field observations and soil investigations were conducted, followed by comprehensive geotechnical analyses and evaluations. Based on these studies, the following conclusions and recommendations were drawn:

• The low modulus clay soil, which is the first layer forming the foundation soil of the grain bins, reaches deeper levels (approximately 6.5m) as it approaches from grain bins S-9 and S-18 to grain bins S-1 and S-10, while it is shallower (approximately 3m) up to grain bins S-2-S-11. In addition, the clay soil shows a thicker trend from S-1 to S-10. The second layer forming the base soil is a high modulus, moderately weathered sandstone with frequent fractures.

• As a result of the geotechnical analyses and calculations, it was determined that they were safe in terms of bearing capacity, horizontal slip, and liquefaction. However, as a result of 2D and 3D analyses and field observations regarding settlement, movement occurred in the area where the clay soil layer was thick, and this movement was found to be intense around 47mm in the vertical direction. It was found that the lack of a drainage system caused settlement due to the softening of the clay soil by surface and rainwater.

• To reduce and control the vertical displacement, a controlled embankment consisting of 1.5m thick GW soil covering the S-1, S-2, S-10, and S-11 grain bins and also 0.80m diameter unreinforced piles covering the S-1 and S-2 grain bins were designed as ground improvement and reinforcement.

• In the case of the soil improvement and reinforcement, the maximum total settlement, maximum differential settlement, and angular distortion obtained for grain bins S-1, S-2, S-10, and S-11 were found to be within the permissible limits. It is also assumed that these settlement values will be lower in reality, since the idealization of the complex soil profile considers the worst case.

• The results of the 2D and 3D stress-deformation analyses are consistent with the field observations, and it is determined that the problem is caused by displacement in the vertical direction. To verify the efficiency of the proposed soil improvement and reinforcement design, a 3D stress-strain analysis was performed. This study has shown that FEM-based software is a simple and advantageous simulation tool for the determination of terrain properties.

• Surface drainage system should be designed to prevent the infiltration and accumulation of surface water and rainwater on the ground surface, especially in the areas where the S-1 and S-10 grain bins are located.

• For future projects involving similar soil conditions and structures, it is recommended that comprehensive soil investigations and proactive soil improvement measures be implemented during the initial design phase. This approach can help mitigate potential settlement issues and ensure the long-term stability and safety of the structures. In addition, regular monitoring and maintenance of drainage systems should be performed to prevent water accumulation and its adverse effects on soil properties.

• Finally, this study highlights the importance of implementing structural health monitoring systems at active facilities. Such systems provide early warnings of undesirable behavior, allowing for timely intervention and prevention of structural damage.

Acknowledgments

The authors gratefully acknowledge the contributions of Hakan Sahin, PhD, PE, for his valuable support in the

editorial review, technical editing, and overall organization of the manuscript.

References

Alekseev, A.G. and Bezvolev. S.G. (2020), "In-situ customization of the helical pile design procedure using plaxis 2D", *Soil Mech. Found. Eng*., **57**, 77-83. https://doi.org/10.1007/s11204-020-09640-9.

Ambily, A.P. and Gandhi, S.R. (2007), "Behavior of stone columns based on experimental and FEM analysis", *J. Geotech. Geoenviron. Eng*., **133**, 405-415. https://doi.org/10.1061/(ASCE)1090-0241(2007)133:4(405).

Banne, S.P., Dhawale, A.W., Patil, R.B., Girase, M., Kulkarni, C., Dake, M. and Khan, S. (2024), "Slope stability analysis of Xanthan gum biopolymer treated laterite soil using plaxis limit equilibrium method (PLAXIS LE)", *KSCE J. Civil Eng*., 1-12. https://doi.org/10.1007/s12205-024-0553-2.

Başköse, Y. and Gökçeoğlu, C. (2019), "An experimental study to compare two soil improvement techniques performance", *Adv. Sci. Technol. Innov*., 265-268. https://doi.org/10.1007/978-3-030-01665-4_61.

Bounds, T.D., Muraleetharan, K.K. and Miller, G.A. (2024), "Lateral Movements of Bridge Embankments on Soft Soils: A Case Study Inspired Investigation", *Geotech. Geol. Eng*., **42**, 121-139. https://doi.org/10.1007/s10706-023-02559-6.

Bowles, E.J: (1996), Foundation analysis and design, 5th Ed., McGraw-Hill, New York

Briancon, L. and Simon, B. (2017), "Pile-supported embankment over soft soil for a high-speed line", *Geosynth. Int*., **24**(3), 293-305. https://doi.org/10.1680/jgein.17.00002.

Can, A., Zengin, B. and Gökçeoğlu, C. (2024), "Comparison of Plaxis-2D and 3D models of improved ground with deep mixing columns", *Eng. Geol. A Habitable Earth*, **4**, 529-542. https://doi.org/10.1007/978-981-99-9069-6_37.

CFEM. (2006), Canadian Foundation Engineering Manual, 4th Edition, Canadian Geotechnical Society, Canada.

Cosgun, T., Öser, C., Erdem, S., Kocak, A. and Sayin, B. (2021), "Material characteristics and stability analysis of gravity stone walls", *Struct. Eng. Int*., **33**(1), 96-106. https://doi.org/10.1080/10168664.2021.1998942.

Çınar, M. (2023), "Investigation of mechanical and physical features of cementitious jet grout applications for various soil types", *Buildings*, **13**(11), 2833. https://doi.org/10.3390/buildings13112833.

Das, B.M. (2011), Principles of Foundation Engineering, SI, 7th Edition, Cengage Learning, Stamford, USA.

Das, B.M. (2019), Advanced Soil Mechanics, 5th Edition, CRC Press, Newyork, USA.

Dias, D. and Grippon, J. (2017), "Numerical modelling of a pile-supported embankment using variable inertia piles", *Struct. Eng. Mech*., **61**(2), 245-253. https://doi.org/10.12989/sem.2017.61.2.000.

Elsawwaf, A., El Sawwaf, M., Nazir, A., Azzam, W., Farouk, A. and Etman, E. (2023), "Consolidation effect on the behavior of micropiled rafts under combined loading: case study", *Arabian J. Sci. Eng*., **48**, 13429-13448. https://doi.org/10.1007/s13369-023-07806-9.

Ergun, M.U. (2023), Principles of soil improvement and strengthening methods, Millimetric Group Printing, Ankara, Türkiye (in Turkish).

Fahmi, K.S., Fattah, M. and Shestakova A. (2018), "Behavior of foundation soil improved by stone column under cyclic load", MATEC Web Conf.239, 05015. https://doi.org/10.1051/matecconf/201823905015.

Hafez, K.M., El Kamash, W.H., Moubarak, A.H. and Kasem, M.A. (2024), "Improvement of soft clay soil using stone columns", Geotechnical Special Publication, **355**, 337-345.

Jamsawang, P., Yoobanpot, N., Thanasisathit, N., Voottipruex, P. and Jongpradist, P. (2016), "Three-dimensional numerical analysis of a DCM column-supported highway embankment", *Comput. Geotech*., **72**, 42-56. https://doi.org/10.1016/j.compgeo.2015.11.006Get.

IdeStatik V10.94. (2020), Static package program manual, Bursa, Türkiye (in Turkish).

IRAP (2021), Kayseri Provincial Disaster Risk Reduction Plan, AFAD Planning and Risk Reduction Department, Kayseri, Türkiye (in Turkish)".

Ketin, İ. (1959), "Orogenic development of Turkey", *J. MTA*, **53**, Ankara.

Kocyigit, A. and Erol, O. (2001), "A tectonic escape structure: Erciyes pull-apart basin, Kayseri, central Anatolia, Turkey", *Geodinamica Acta*, **14**(1-3), 133-145. https://doi.org/10.1080/09853111.2001.11432439.

Kumar, N. and Kumar, R. (2025), "Performance of geosynthetic-encased stone columns in sandy soils subjected to vertical cyclic loads", *Int. J. Geomech*., **25**(1). https://doi.org/10.1061/IJGNAI.GMENG-10283.

Mishra, B.A. (2016), "A study on ground improvement techniques and its applications", *Int. J. Innov. Res. Sci. Eng. Tech*., **5**(1), India.

Nicholson, P.G. (2015), Soil Improvement and Ground Modification Methods, Elseveir, Amsterdam.

Nikolay, M., Kiyota, T., Osawa, S. and Numata, A. (2024), "State-of-the-art application of the log-piling method in the role of shallow ground improvement for liquefaction mitigation", *Arch. Tech. Sci*., **30**, 59-78. https://doi.org/10.59456/afts.2024.1630.059M.

Özlü, T., Gündüz, S. and Çağlak, S. (2017), "Geomorphology of Tuzla Lake Basin, Kayseri", February 28, Studies of The Ottoman Domain. 7(12). https://ssrn.com/abstract=3044365.

Özlü, T. and Gündüz, S. (2018), "Hydrographic characteristics of Tuzla Lake (Kayseri) and its level changes between", **28**(1), 1975-2015, Fırat University Journal of Social Sciences.

PLAXIS 2D (2023), Reference Manual, Bentley, Delft, The Netherlands.

PLAXIS 3D (2023), Reference Manual, Bentley, Delft, The Netherlands.

Rao, S.S. (2011), The Finite Element Method in Engineering, 5th Ed., Elseveir.

Potts, D.M. and Zdravkovic, L. (1991), Finite element analysis in geotechnical engineering: Theory, Thomas Telford, London.

Potts, D.M. and Zdravkovic, L. (2001), Finite element analysis in geotechnical engineering: Application, Thomas Telford, London.

Sivrikaya, O. (2021a), Foundation Construction in Civil Engineering I, Birsen Publishing House, Istanbul, Türkiye (in Turkish).

Sivrikaya, O. (2021b), Foundation Construction in Civil Engineering II, Birsen Publishing House, Istanbul, Türkiye (in Turkish).

Sondermann, W. (2018), "Ground improvement as alternative to piling-effective design solutions for heavily loaded structures", Latest Thoughts on Ground Improvement Techniques, 1-25, 24-28 November, Cairo, Egypt. https://doi.org/10.1007/978-3-030-01917-4_1.

Tatar, O., Piper, J.D.A. and Gürsoy, H. (2000), "Palaeomagnetic study of the erciyes sector of the ecemis fault zone: Neotectonic deformation in the southeastern part of the anatolian block", Geological Society London Special Publications, **173**(1), 423-440. https://doi.org/10.1144/GSL.SP.2000.173.01.20.

TBEC (2018), Turkish Building Earthquake Code, Provincial Disaster and Emergency Directorate (AFAD), Ankara, Türkiye.

Tipsunavee, T., Arangjelovski, G. and Jongpradist, P. (2023), "Numerical analysis on effects of soil improvement on pile forces on existing high-rise building", *Buildings*, **13**(6). https://doi.org/10.3390/buildings13061523.

Umaiyan, U. and Muthukkumaran, K. (2022), "Numerical study on the effect of using dented sheet liner in pervious concrete pile to improve soft soil", *Int. J. Geomech*., **22**(9). https://doi.org/10.1061/(ASCE)GM.1943-5622.0002482.

Uncuoglu, E., Latifoglu, L. and Kaya, Z. (2023), "A hybrid approach to predict the bearing capacity of a square footing on a sand layer overlying clay", *Geomech. Eng*., **34**(5), 561-575. https://doi.org/10.12989/gae.2023.34.5.561.

URL-1 http://www.koeri.boun.edu.tr/sismo/zeqdb/default.asp, 20.02.2024.

Wang, C., Wang, H., Qin, W., Wei, S., Tian, H. and Fang, K. (2023), "Behaviour of pile-anchor reinforced landslides under varying water level, rainfall, and thrust load: Insight from physical modelling", *Eng. Geol*., **325**, 107293. https://doi.org/10.1016/j.enggeo.2023.107293.

Xiao, J., Luo, Z., Martin II, J. R., Gong, W. and Wang, L (2016), "Probabilistic geotechnical analysis of energy piles in granular soils", *Eng. Geol*., **209**, 119-127. https://doi.org/10.1016/j.enggeo.2016.05.006.

Vanni, D., Bertero, A., Attala, D., Malavolta, M., Marchi, G., Marchi, M., Ragazzini, A. and Samori, L. (2018), "Urban renovation of the new marina in Rimini: Displacement piles as soil improvement and settlement reduction for the construction of a new dwelling and business centre", *Proceedings of the 5th International symposium on deep foundations on bored and auger piles (BAP V)*, Ghent, Belgium, 8-10 September.

Varaksin, S., Hamidi, B., Huybrechts, N. and Denies, N. (2016), "Ground improvement vs. pile foundations", ISSMGE - ETC 3 *Proceedings of the International Symposium on Design of Piles in Europe*, Leuven, Belgium, 28-29 April

Vesic, A.S. (1973), "Analysis of ultimate loads of shallow foundations", *J. Soil Mech. Found. Division*, **99**(1), 45.

Vesic, A.S. (1975), Bearing Capacity of Shallow Foundations, Foundation Engineering Handbook, 1st edition, Winterkorn H.F. and Fang H.Y. (Editors), Chapter 3, Galgotia Booksource, New Delhi.

Yao, Y., Shi, X.F. and Han, D.D. (2024), "Lateral effects of jet grouting on surrounding soil and circular diaphragm walls", *Buildings*, **14**(11). https://doi.org/10.3390/buildings14113587.

Yazici, M.F. and Keskin, S.N. (2021), "Optimum design of multi-anchored larssen type sheet pile wall for temporary construction works", *Geomech. Eng*., **27**(1). https://doi.org/10.12989/gae.2021.27.1.001.

Zhang, B., Liu, H.L. and Chu, J.A. (2010), "Analysis of stress distribution in large diameter concrete pipe pile supported embankment", *Proceedings of the 1st International Symposium on Ground Improvement Technologies and Case Histories*, 239-246.

Zhao, L., Chen, Y., Chen, W., Wang, J. and Ren, C. (2023), "The performance of T-shaped deep mixed soil cement column-supported embankments on soft ground", *Constr. Build. Mater*., **369**, 130578. https://doi.org/10.1016/j.conbuildmat.2023.130578.

Zhao, Y., Gong, W., Ling, X., Li, P., Wang, Z. and Fan, H. (2021), "Model test on the vibration reduction characteristics of a composite foundation with gravel cushion under different seismic wave amplitudes", *Shock Vib*., **2021**(1), 6696031. https://doi.org/10.1155/2021/6696031.